analytical chemistry

pubs.acs.org/ac Article

Addressable Label-Free Photoelectric Sensor Array with Self-Calibration for Detection of Neuron Specific Enolase

Zhenyuan Xing, Shuo Zhang, Huan Wang,* Hongmin Ma, Dan Wu, Dawei Fan, Xiang Ren, Qin Wei,* and Huangxian Ju

Cite This: *Anal. Chem.* 2022, 94, 6996−7003 Read Online

ACCESS | Metrics & More | Article Recommendations | Supporting Information

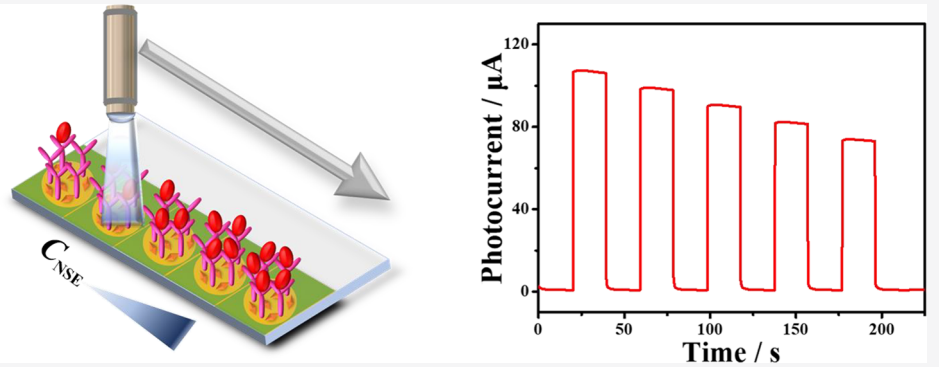

ABSTRACT: An addressable label-free photoelectric immunosensor array was designed for detection of neuron specific enolase (NSE) based on TiO_2/CdS as substrate materials. In this work, the hydrothermal synthesized TiO_2 nanorod film is evenly grown on the surface of the fluorine-doped tin oxide (FTO), and then CdS with a narrow band gap is added for sensitization through successive ionic layer adsorption reactions. The obtained TiO_2/CdS composite materials with matched energy band structures promote the rapid electron transfer and effectively reduce the recombination of electron hole pairs, which greatly enhance the visible light absorption and increased photocurrent intensity. In order to construct a suitable sensor array, the sensitized FTO electrode is divided into multiple regions of equal size by insulating stickers, and then the addressable and continuous detection of multiple samples can be achieved. Because multiple detection regions are prepared and tested under the same conditions, the difference effectively reduces, and the sensor can realize self-calibration and obtain more accurate results. Under optimal conditions, this sensor array can detect NSE in the linear range of 0.01−100 ng mL^{-1} with a detection limit of 2.49 pg mL^{-1} (S/N = 3). The sensor array has good selectivity, stability, and reproducibility, making it a viable approach for real sample detection.

INTRODUCTION

People have heightened expectations for detection technologies with high sensitivity and universality in recent years, particularly when health, safety, and environmental problems occur frequently and receive more attention.[1,2] Combining photoelectrochemical technology and bioanalysis technology, photoelectrochemical (PEC) immunoassay technology is an emerging method for detection of various trace biomarkers, such as tumor markers, disease antigens, and even cancer cells.[3,4] Thanks to the characteristics of photoactive materials and the miniaturization of analytical equipment, photoelectric immunoassays have the advantages of fast response, low background signal, and high sensitivity. Therefore, many sensing platforms with high sensitivity and selectivity have been developed.[5−8]

In order to improve the detection efficiency, developing a high-throughput, multichannel PEC biosensor is necessary. Up until now, a variety of multichannel PEC biosensors for biological analysis have been developed. They can be divided into three modes. One is single electrode mode, which produces different current signals by using photoactive substances to respond to different wavelengths[9] or external bias voltage,[10,11] so as to achieve the purpose of separate detection. The second mode is combined electrode array mode,[12−14] which combines several independent working electrodes and uses a multichannel electrochemical workstation for simultaneous detection. The third mode is the regional electrode array mode,[15,16] which divides the large-area working electrode into several detection areas and controls the light source to irradiate the detection area in turn to realize

Received: December 27, 2021
Accepted: April 25, 2022
Published: May 5, 2022

https://doi.org/10.1021/acs.analchem.1c05577
Anal. Chem. 2022, 94, 6996−7003

Scheme 1. Preparation Process of the Proposed PEC Immunosensor Array

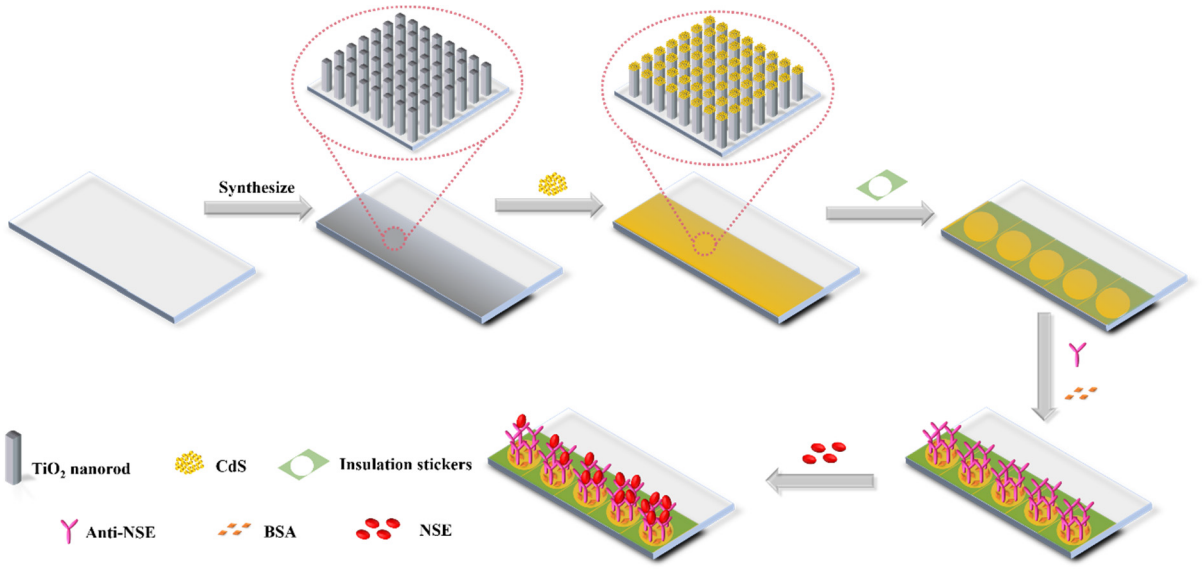

continuous detection. Compared with the second mode, the regional electrode array is located on the same electrode, which could reduce the differences of the electrodes, and at the same time, the same preparation and test conditions provide a possibility for self-calibration. These characteristics make the regional electrode array an ideal scheme for the construction of multichannel PEC biosensors.

The photoelectric activity of materials is essential for improving sensor array performance. Because of their good photoelectric activity, high stability, and low cost, metal oxide semiconductors, such as ZnO,[17,18] WO_3,[19] TiO_2,[20,21] are frequently utilized materials in the field of photoelectric sensing and photocatalysis. While, in order to control the difference of regions on the electrode array, the uniformity of material distribution on the electrode is very important. Due to the polarization effect or coffee ring effect, commonly used electrode modification methods, such as the electrodeposition method,[22,23] anodic oxidation method,[24,25] spin coating method,[26,27] drop method,[28,29] and so on, are difficult to ensure the uniformity of the material on the electrode, especially for the large area array electrode. As a result, the photocurrent difference is obvious, and the reproducibility is poor.[30,31] To meet the uniformity of materials, in situ growth of materials may be a good solution.

Many researchers prefer TiO_2 nanorod arrays produced on FTO in situ because of their high order, large specific surface area, and higher adsorption capacity.[32−34] However, TiO_2 has a wide band gap, making it susceptible to carrier recombination and the absorption and use of visible light is limited. Thus, it is required to combine with narrow-band semiconductors to reform the usage of visible light[35] and decrease carrier recombination. While, as a typical narrow band gap semiconductor, CdS has high visible light absorption[36] and is commonly utilized in the fabrication of heterojunctions to boost conversion efficiency.[37,38]

Neuron specific enolase (NSE) is found naturally in a variety of nerve and neuroendocrine tissues. The concentration of NSE in serum rises significantly in patients with small cell lung cancer, neuroblastoma, or chemotherapy. As a tumor marker with high specificity, the rapid and reliable detection of NSE is critical for illness diagnosis and timely detection of diagnosis and treatment outcomes.[39,40] In this study, homogeneous and dense TiO_2 nanorod films were produced in situ on the surface of FTO and TiO_2 was sensitized by CdS. The TiO_2/CdS composite materials can help to separate electrons and holes and increase visible light utilization. The large-area electrode was divided into several small detection regions by insulating stickers. Through the test of each region, the regional electrode array with self-calibration function was successfully constructed and realized a more accurate detection of NSE.

EXPERIMENTAL SECTION

Reagents and Apparatus. Details of the reagents and apparatus are included in the Supporting Information.

Preparation of the TiO_2 Nanorods. First, FTO glass (5 cm × 2.5 cm) was cleaned with cleaning agent, acetone, ethanol, and deionized water and then dried in a special oven. TiO_2 nanorods were synthesized on FTO glass substrate according to previous reports[41,42] with little change. In the typical synthesis process, 15 mL of water, 15 mL of hydrochloric acid, and 0.5 mL of tetrabutyl titanate were mixed and fully stirred over 30 min, and then a clear and transparent solution was obtained. The conductive surface of the FTO glass substrate was placed against the Teflon lining at an angle of 45° downward. The previously prepared solution was poured into the lining and reacted for 9 h at 160 °C. After cooling to room temperature, the FTO glass was removed and cleaned with ultrapure water. When it was dry, it was annealed at 350 °C for 1 h in a muffle furnace.

Preparation of the FTO/TiO_2/CdS Photoelectrode. The CdS sensitization layer was loaded on the surface of the TiO_2 film by a successive ionic layer adsorption reaction. First, a 0.1 mol L^{-1} solution of $Cd(NO_3)_2$ labeled as solution A and a 0.1 mol L^{-1} solution of Na_2S labeled as solution B were prepared with ultrapure water. The prepared TiO_2 film was immersed in solution A, and after 30 s, it was removed and washed with ultrapure water, then immersed in the solution B for another 30 s. These two steps were called a cycle, and the cycle was repeated 5 times. Finally, it was cleaned with ultrapure water and dried.

Fabrication of the PEC Immunosensor. First, the prepared electrode was divided into five regions of the same

https://doi.org/10.1021/acs.analchem.1c05577
Anal. Chem. 2022, 94, 6996−7003

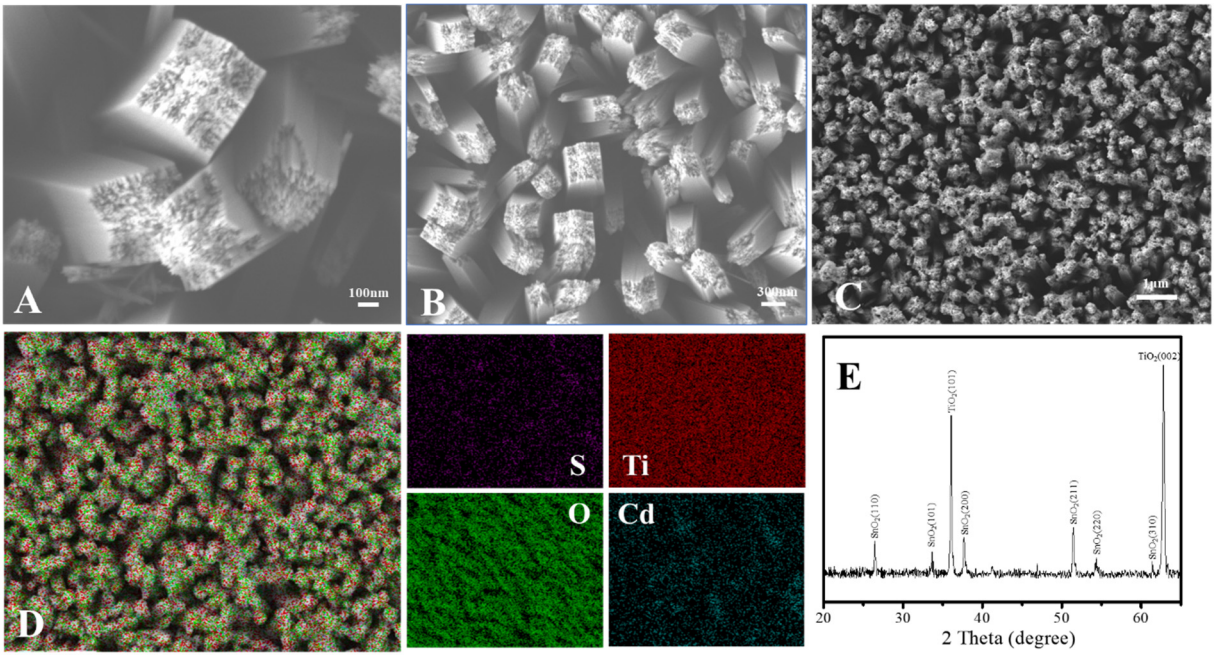

Figure 1. SEM images of (A) and (B) TiO_2 nanorods, (C) TiO_2/CdS, and (D) EDS spectrum of TiO_2 nanorods, and (E) XRD of TiO_2 nanorods.

size by insulating stickers. Then, the photocurrent signals of five regions are tested and recorded, respectively. The test value shall be used as the reference value for self-calibration. Each region added by 4 μL of thioglycolic acid, then dried, and rinsed with ultrapure water to modify the −COOH group on the CdS surface. Then, 5 μL of a mixed solution of 10 mmol L^{-1} EDC and 2 mmol L^{-1} NHS was incubated on different regions of the electrode to activate the −COOH group. Then 6 μL of 5 μg mL^{-1} antibody (Ab) was added to each region and incubated at 4 °C for 3 h. Subsequently, the electrode was cleaned with phosphate buffered saline (PBS) to remove the unattached Ab. Next, 5 μL of 1 wt % bovine serum albumin (BSA) solution was added to each region to block the nonspecific binding sites. Finally, different concentrations of NSE were added to different region and incubated at 4 °C for 1 h. At last, the electrode was cleaned with PBS, and the photoelectric sensor array was successfully constructed. By controlling the lighting position in the PEC test, the light can illuminate each region in turn, realizing continuous detection. The preparation process of the PEC sensor array is shown in Scheme 1.

PEC Detection. The PEC test was carried out in PBS (pH = 7.4) solution containing 0.3 mol L^{-1} ascorbic acid. The wavelength of the test light source is 420−430 nm and the power is 10 W cm^{-2}. The photocurrent was measured using an electrochemical workstation, and i−t curves were recorded.

RESULTS AND DISCUSSION

Characterization of Synthetic Materials. The synthesized TiO_2 and CdS were characterized by scanning electron microscope (SEM), energy dispersive spectrum (EDS), elemental distribution methods, and X-ray power diffraction (XRD). TiO_2 nanorods grow virtually vertically on the FTO substrate, and the nanorods are square and have a smooth surface with a diameter of about 300 nm as illustrated in Figure 1A,B. Moreover, the uniform distribution of substrate materials is a prerequisite for providing similar PEC background signals. Thus, we took a large-scale SEM image to verify the uniformity

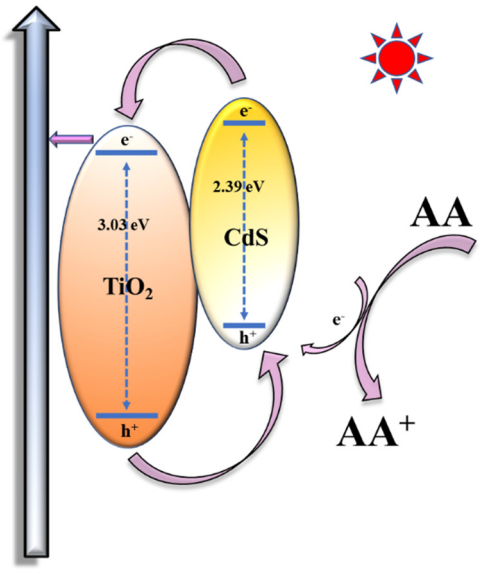

Figure 2. Proposed mechanism for the photocurrent response.

of the TiO_2 nanorod distribution. TiO_2 nanorod films are evenly distributed on the substrate and almost in the same plane without damage from stacking (Figure S1). The nanorods retain their morphology after modification with CdS, but their surfaces become rough (Figure 1C). Furthermore, the distribution of CdS on TiO_2 nanorods is uniform, and no agglomeration formation is observed. CdS has been successfully changed on the surface of the TiO_2 nanorods, which can be observed from the EDS mapping (Figure 1D). Figure 1E is the XRD pattern of FTO/TiO_2. It can be seen from the figure that, except for the SnO_2 diffraction peaks of the FTO substrate, there are only two rutile phase TiO_2 (101) and (002) diffraction peaks, at 2θ = 36.08° and 62.79°, respectively. The absence of only two characteristic peaks and other peaks of the rutile phase indicates that the nanorods are single crystals.

https://doi.org/10.1021/acs.analchem.1c05577
Anal. Chem. 2022, 94, 6996−7003

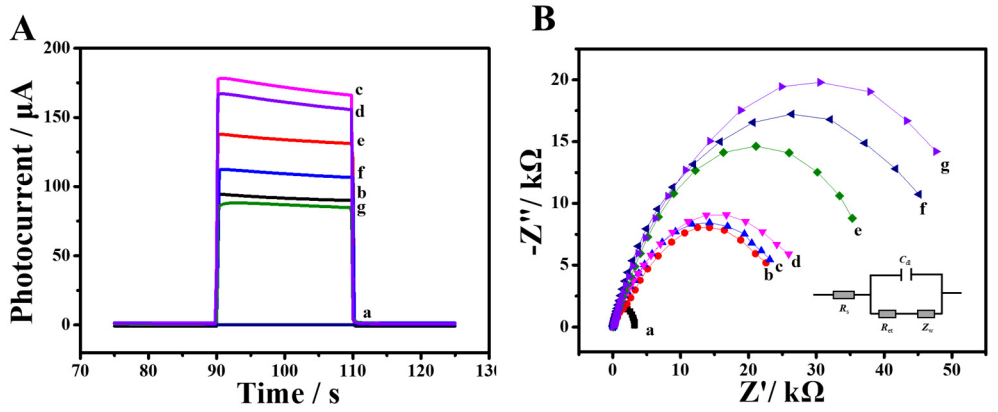

Figure 3. (A) PEC signal and (B) EIS Nyquist plots of (a) FTO, (b) FTO/TiO_2, (c) FTO/TiO_2/CdS, (d) FTO/TiO_2/CdS/EDC-NHS, (e) FTO/TiO_2/CdS/EDC-NHS/Ab, (f) FTO/TiO_2/CdS/EDC-NHS/Ab/BSA, and (g) FTO/TiO_2/CdS/EDC-NHS/Ab/BSA/NSE (c_{NSE} = 1 ng mL^{-1}). The applied voltage is 0 V.

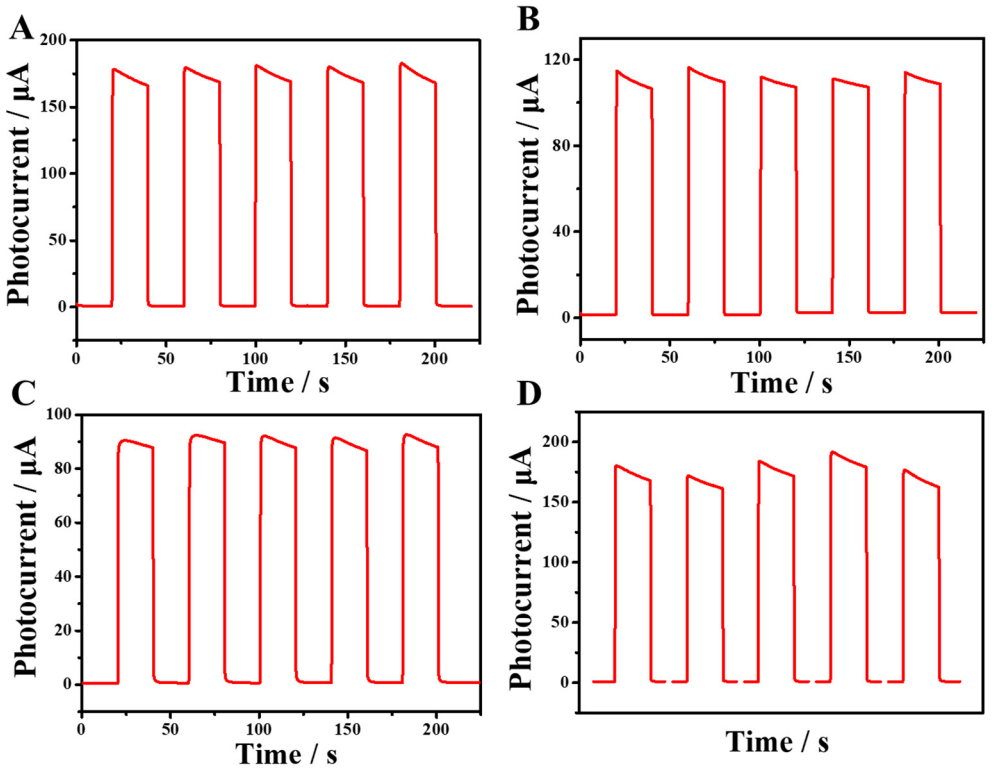

Figure 4. (A) Photocurrent signal at different regions of FTO/TiO_2/CdS. (B) Photocurrent signal at different regions of FTO/TiO_2/CdS/EDC-NHS/Ab/BSA. (C) Photocurrent signal at different regions of FTO/TiO_2/CdS/EDC-NHS/Ab/BSA/NSE (c_{NSE} = 1 ng mL^{-1}). (D) Photocurrent signal at five different batches of FTO/TiO_2/CdS. The applied voltage is 0 V.

Mechanism Exploration. The transfer mechanism of photogenerated electrons and holes in the AA solution is shown in Figure 2. TiO_2 and CdS have different band gaps and light absorption wavelengths, but their energy levels are matched.[43] The electron of CdS on the valence band (VB) transfers to the conduction band (CB) under light illumination; then it smoothly gets into the CB of TiO_2, and subsequently, the remaining electrons after combination are collected and transferred to the FTO substrate, thus the photocurrent is formed. At the same time, AA in the solution as the electron donor will be oxidized and lose electrons; consequently, the holes generated in the process will be refilled. On this basis, antibody and antigen modified on the electrode surface will hinder the electron transfer process and decrease the photocurrent signal. As the concentration of the detected NSE increases, the blocking effect increases, realizing the quantitative detection of NSE.

Performance Characterization of Photoelectric Sensor Array. Figure 3A is a graph of the layer-by-layer modified photocurrent when the photoelectrode turns on and off with time. The photocurrent signal of bare FTO is very weak and can be ignored, as seen in the figure. When TiO_2 nanorods grow on the surface, the photocurrent signal increases to about 90 μA. When the surface is modified with CdS, the photocurrent increases to 170 μA. When Ab is bound on the surface of the electrode, the photocurrent signal decreases to 133 μA because Ab obstructs electron transmission. After using

https://doi.org/10.1021/acs.analchem.1c05577
Anal. Chem. 2022, 94, 6996−7003

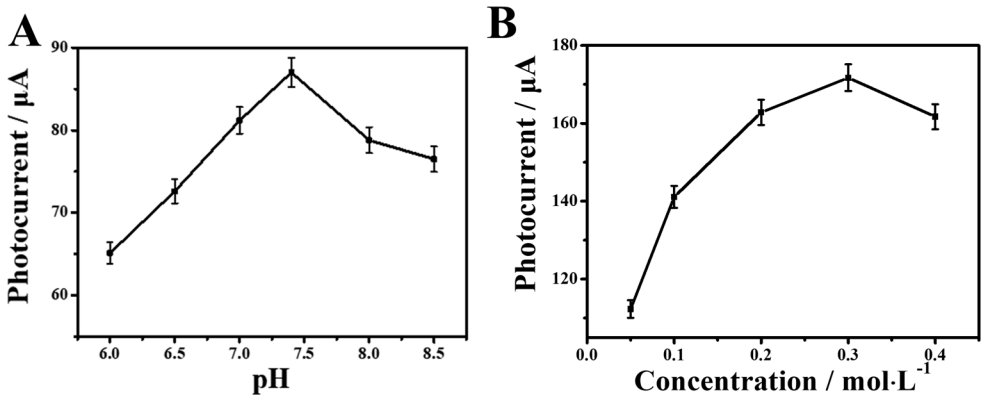

Figure 5. (A) pH and (B) AA concentrations (c_{NSE} = 1 ng mL^{-1}, error bars = SD, n = 3).

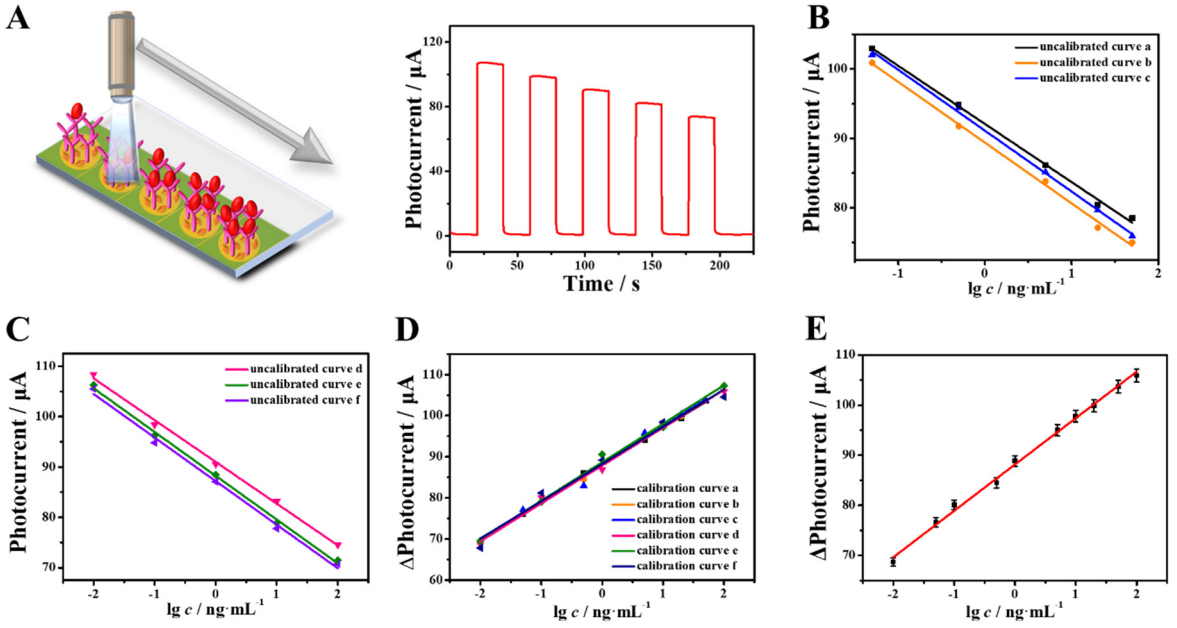

Figure 6. (A) Sensor array detection process schematic and photocurrent of the immunosensor of NSE (0.01, 0.1, 1, 10, 100 ng mL^{-1}). (B) Uncalibrated curves. The concentrations at each point of curves a, b, and c are 0.05, 0.5, 5, 20, and 50 ng mL^{-1}. (C) Uncalibrated curves. The concentrations at each point of curves d, e, and f are 0.01, 0.1, 1, 10, and 100 ng mL^{-1}. (D) Calibrated curve. (E) Corresponding calibration curve.

Table 1. Developed PEC Immunosensors for Detecting NSE Compared to Other Published Immunosensors

method	linear range	detection limit	refs
electrochemical immunoassay	0.1−200 ng mL^{-1}	0.04 ng mL^{-1}	44
fluorescence immunosensor	5−50 ng mL^{-1}	42.6 pg mL^{-1}	45
electrochemical immunosensor	1−1000 ng mL^{-1}	0.3 ng mL^{-1}	46
PEC immunosensor	75−723 ng mL^{-1}	0.12 ng mL^{-1}	4
PEC immunosensor	0.1−1000 ng mL^{-1}	0.05 ng mL^{-1}	47
PEC immunosensor	0.1 pg mL^{-1}−50 ng mL^{-1}	1.57 fg mL^{-1}	48
PEC immunosensor array	0.01−100 ng mL^{-1}	2.49 pg mL^{-1}	this work

BSA to block nonspecific binding sites and binding to NSE, the photocurrent signal further decreased for the same reason.

Electrochemical impedance spectroscopy (EIS) is an important means to characterize the interface characteristics of PEC sensors. The layer-by-layer modified PEC sensor was characterized in a test solution containing 5.0 mmol L^{-1} $[Fe(CN)_6]^{3-/4-}$ and 0.10 mol L^{-1} KCl. As shown in Figure 3B, the bare FTO has only a small resistance (curve a). Curve b is the resistance of TiO_2 nanorods grown on the surface, and the resistance is significantly higher than that of a. Curves c, d, e, and f are modified with CdS, EDN-NHS, Ab, BSA, and NSE, respectively, and it can be seen that the resistance increases successively, which proves the successful layer by layer modification of the immunosensor.

In order to certify the relationship between crosstalk interference and the distance between the two adjacent electrodes, we numbered the five regions of the electrode array as A, B, C, D, and E from left to right. Region C was used as a reference, and it was tested before and after removing A, E, B, and D in turn. As can be seen from Figure S2, with the successive removal of A, E, B, and D, the detection signal of region C decreased by 0.48%, 0.81%, 1.5%, and 2.3%, respectively. We speculate that this phenomenon is caused by the reduction of the electrode interface, and the low background signals in the corresponding regions are missing. Anyway, the influence is still extremely low, so there is almost no crosstalk signal.

https://doi.org/10.1021/acs.analchem.1c05577
Anal. Chem. 2022, 94, 6996−7003

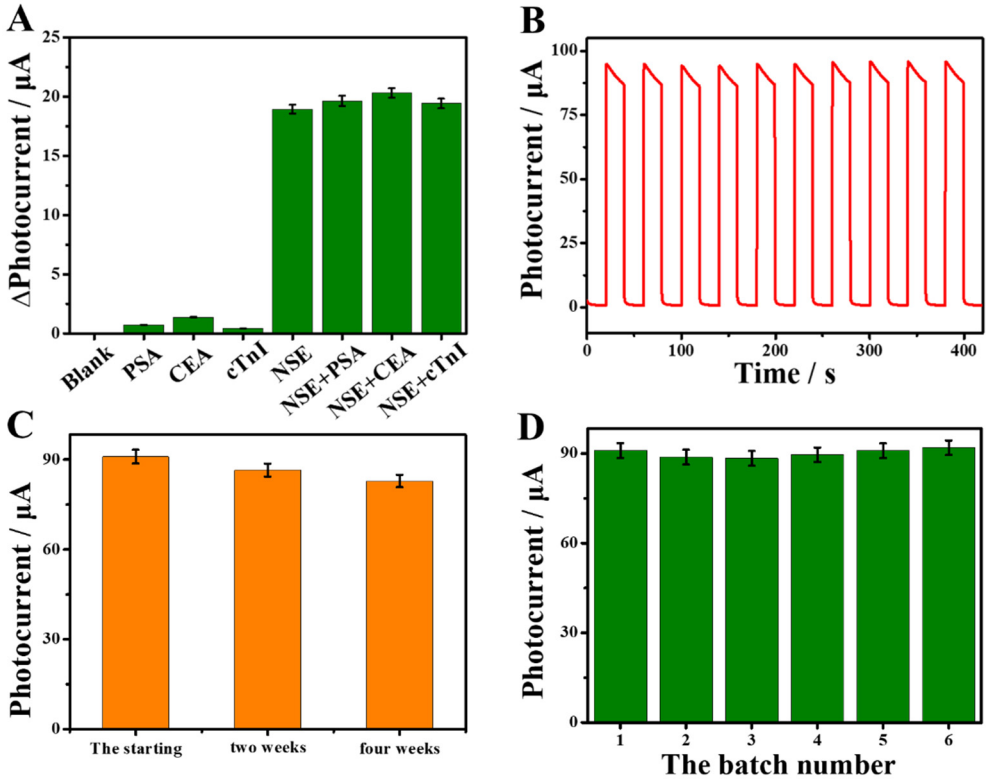

Figure 7. (A) Selectivity of the immunoassay (c_{NSE} = 1 ng mL^{-1}, error bars = SD, n = 3). (B) Stability of the immunoassay. (C) Photocurrent signal changes with storage time. (D) Reproducibility of the proposed PEC immunosensor (error bars = SD, n = 3).

Table 2. Serum Sample Recovery Experiment

initial (ng mL^{-1})	addition contents (ng mL^{-1})	detection content (ng mL^{-1})	average value (ng mL^{-1})	RSD (%)	recovery (%)
	0.100	2.137, 2.083, 2.074, 2.123, 2.094	2.102	1.3	94.0
2.008	1.000	3.136, 3.010, 2.877 3.028, 3.009	3.012	3.1	101.2
	10.00	13.04, 11.94, 12.01, 11.91, 12.30	12.24	3.9	102.3

There may be uneven distribution of photoactive materials and inconsistent binding conditions when incubating the antigen and antibody on different regions of the sensor array, which will cause excessive signal differences between the regions and affect the final detection result. Therefore, it is necessary to verify the differences of the five regions on every layer. As seen from Figure 4, the differences of the five regions are little whether on FTO/TiO_2/CdS (Figure 4A), FTO/TiO_2/CdS/EDC-NHS/Ab/BSA (Figure 4B), or FTO/TiO_2/CdS/EDC-NHS/Ab/BSA/NSE (Figure 4C), and the relative standard deviations (RSD) of the three layers are 0.66%, 1.22%, and 0.89%, respectively. At the same time, the differences of signals between the different electrode batches were compared, as shown in the Figure 4D, and the RSD of the five different batches is 3.22%. These results suggest that the regional array can indeed reduce the measurement error and get the more accurate results. In addition, the stability and long-term storage test of the substrate material are also carried out. As shown in Figure S3, the substrate material shows excellent stability.

Optimization of Experimental Conditions. In order to obtain the best performance of the sensor, the experimental conditions have been optimized. During the test, the pH of the solution and the concentration of AA in the solution were optimized. Figure 5A shows that when the pH value increased, the photocurrent signal gradually increased and peaked at pH 7.4. The effect of AA concentration on sensor performance is shown in Figure 5B. The photocurrent signal grew and reached a maximum when the AA concentration was increased from 0.05 mol L^{-1} to 0.3 mol L^{-1}. As a result, the electrolytic solution used was PBS (pH 7.4) with 0.3 mol L^{-1} AA.

Analysis Performance. Under the best experimental conditions, the different regions of the electrode array were modified with different concentrations of NSE, and then the light source was moved to irradiate the different detection regions in sequence, as shown in Figure 6A. Due to the batch differences of the sensor arrays, the fabrication curves obtained from different arrays are different, as shown in Figure 6B,C. Therefore, making a calibration is helpful to obtain an accurate result. Since the initial photocurrent signals of the five regions were recorded, the differences between the detection signals and their initial signals can be used for self-calibration. After calibration, the difference between different batches is significantly reduced, and the fabrication curves come closest to coinciding. The difference between the reference value and the detection signal has a linear relationship with the logarithm of NSE concentration, as shown in Figure 6E. As a result, when the NSE concentration increases from 0.01 ng mL^{-1} to 100 ng mL^{-1}, the photocurrent signal changes gradually increased. The linear regression equation of the correction curve is I = 87.9 + 9.2 × lg c, and the limit of detection is 2.49 pg mL^{-1}. In addition, the detection limit and detection range of this sensor

https://doi.org/10.1021/acs.analchem.1c05577
Anal. Chem. 2022, 94, 6996−7003

array were compared with other sensors in detail (Table 1), and it can be seen that this sensor array has acceptable performance in NSE detection.

In order to certify the selectivity of the sensor array, 1 ng mL^{-1} of NSE were used as reference and 10 ng mL^{-1} of PSA, CEA, and cTnI were used as interfering substances for comparison. As seen from Figure 7A, only NSE showed an obvious photocurrent change, and the addition of 10-fold concentration of interfering substances still could not cause an obvious change compared with the addition of only NSE, suggesting that the sensor array has good selectivity. The stability test was carried out for continuous testing of 480 s, and the lamp was switched on and off 10 times. The photocurrent signal is almost unchanged, indicating that the array sensor has a stable response to NSE (Figure 7B). Moreover, the prepared sensor array was stored at 4 °C for 4 weeks for a long-term stability test. As shown in the Figure 7C, after 2 weeks, the test signal is 95.05% of the initial signal, and 4 weeks later, the test signal is 90.4% of the initial signal, suggesting the sensor array has good stability. The reproducibility of the array sensor was verified by detecting the photocurrent signals of six different batches of array sensors. As shown in Figure 7D, when the NSE concentration was 1 ng mL^{-1}, the RSD of the 6 sensor arrays was 1.85%, suggesting the reproducibility is also good.

Real Sample Analysis. Different concentrations of NSE standard solutions were added to the serum samples to test the application of the sensor in actual situations (Table 2). The RSDs of the prepared sensor were less than 3.9, and the recovery rates were from 94.0% to 102.3%. It can be seen that the constructed sensor is sensitive and accurate for NSE detection and can be applied to actual sample analysis.

CONCLUSION

In conclusion, a new PEC immunosensor array was developed for sensing of NSE using TiO_2/CdS composites as the substrate. TiO_2/CdS with a larger specific surface area and higher conversion efficiency were prepared and evenly distributed on the surface of FTO. After dividing the TiO_2/CdS modified electrode into different test regions, it can provide almost the same photocurrent signals. Moreover, the signal difference between batches can be significantly reduced after simple self-calibration. The successfully constructed PEC sensor array has the characteristics of accuracy and convenience. It can detect NSE quickly and sensitively, with good selectivity, reproducibility, and stability. Moreover, a wide detection range and a low detection limit was obtained. It offers a practical method for detecting neuron-specific enolase in the clinic as well as a design concept for photoelectric sensor arrays.

ASSOCIATED CONTENT

Supporting Information

The Supporting Information is available free of charge at https://pubs.acs.org/doi/10.1021/acs.analchem.1c05577.

Reagents, apparatus, TiO_2 nanorod SEM image at a large scale, crosstalk verification between different regions, and stability test of the CdS/TiO_2 electrode (PDF)

AUTHOR INFORMATION

Corresponding Authors

Huan Wang − *Collaborative Innovation Center for Green Chemical Manufacturing and Accurate Detection, Key Laboratory of Interfacial Reaction & Sensing Analysis in Universities of Shandong, School of Chemistry and Chemical Engineering, University of Jinan, Jinan 250022 Shandong, P.R. China;* orcid.org/0000-0002-0855-1427; Phone: +86 531 82760510; Email: wanghuan8711@163.com

Qin Wei − *Collaborative Innovation Center for Green Chemical Manufacturing and Accurate Detection, Key Laboratory of Interfacial Reaction & Sensing Analysis in Universities of Shandong, School of Chemistry and Chemical Engineering, University of Jinan, Jinan 250022 Shandong, P.R. China;* orcid.org/0000-0002-3034-8046; Email: sdjndxwq@163.com

Authors

Zhenyuan Xing − *Collaborative Innovation Center for Green Chemical Manufacturing and Accurate Detection, Key Laboratory of Interfacial Reaction & Sensing Analysis in Universities of Shandong, School of Chemistry and Chemical Engineering, University of Jinan, Jinan 250022 Shandong, P.R. China*

Shuo Zhang − *Collaborative Innovation Center for Green Chemical Manufacturing and Accurate Detection, Key Laboratory of Interfacial Reaction & Sensing Analysis in Universities of Shandong, School of Chemistry and Chemical Engineering, University of Jinan, Jinan 250022 Shandong, P.R. China*

Hongmin Ma − *Collaborative Innovation Center for Green Chemical Manufacturing and Accurate Detection, Key Laboratory of Interfacial Reaction & Sensing Analysis in Universities of Shandong, School of Chemistry and Chemical Engineering, University of Jinan, Jinan 250022 Shandong, P.R. China;* orcid.org/0000-0002-7061-8944

Dan Wu − *Collaborative Innovation Center for Green Chemical Manufacturing and Accurate Detection, Key Laboratory of Interfacial Reaction & Sensing Analysis in Universities of Shandong, School of Chemistry and Chemical Engineering, University of Jinan, Jinan 250022 Shandong, P.R. China;* orcid.org/0000-0002-8732-5988

Dawei Fan − *Collaborative Innovation Center for Green Chemical Manufacturing and Accurate Detection, Key Laboratory of Interfacial Reaction & Sensing Analysis in Universities of Shandong, School of Chemistry and Chemical Engineering, University of Jinan, Jinan 250022 Shandong, P.R. China*

Xiang Ren − *Collaborative Innovation Center for Green Chemical Manufacturing and Accurate Detection, Key Laboratory of Interfacial Reaction & Sensing Analysis in Universities of Shandong, School of Chemistry and Chemical Engineering, University of Jinan, Jinan 250022 Shandong, P.R. China;* orcid.org/0000-0002-4321-4282

Huangxian Ju − *State Key Laboratory of Analytical Chemistry for Life Science, Department of Chemistry, Nanjing University, Nanjing 210023, P.R. China;* orcid.org/0000-0002-6741-5302

Complete contact information is available at: https://pubs.acs.org/10.1021/acs.analchem.1c05577

https://doi.org/10.1021/acs.analchem.1c05577
Anal. Chem. 2022, 94, 6996−7003

Notes

The authors declare no competing financial interest.

■ ACKNOWLEDGMENTS

This study was financially supported by the National Natural Science Foundation of China (Grant No. 21777056), Special Foundation for Taishan Scholar Professorship of Shandong Province, Shandong Provincial Natural Science Foundation (Grants ZR2020YQ13 and ZR2020QB097), a Project of Shandong Province Higher Educational Youth Innovation Science and Technology Program (Grant 2020KJC008), and Jinan Scientific Research Leader Workshop Project (Grant 2020GXRC048).

■ REFERENCES

(1) Zhao, W. W.; Xu, J. J.; Chen, H. Y. *Chem. Soc. Rev.* **2015**, *44* (3), 729−741.
(2) Zhang, X. R.; Liu, M. S.; Liu, H. X.; Zhang, S. S. *Biosens. Bioelectron.* **2014**, *56*, 307−312.
(3) Fan, B. B.; Fan, Q.; Cui, M.; Wu, T. T.; Wang, J. S.; Ma, H. M.; Wei, Q. *ACS Appl. Mater. Interfaces.* **2019**, *11* (27), 24764−24770.
(4) Soomro, R. A.; Kalwar, N. H.; Avci, A.; Pehlivan, E.; Hallam, K. R.; Willander, M. *Biosens. Bioelectron.* **2019**, *141*, 111331.
(5) Wang, Y. Y.; Yin, L.; Wu, J.; Li, N.; He, N.; Zhao, H. X.; Wu, Q.; Li, X. T. *Ceram. Int.* **2021**, *47* (21), 29807−29814.
(6) Yang, W. K.; Wang, X. H.; Hao, W. J.; Wu, Q.; Peng, J.; Tu, J. C.; Cao, Y. *J. Mater. Chem. B* **2020**, *8* (11), 2363−2370.
(7) Chen, D. L.; Zou, X.; Dong, F.; Zhen, C.; Xiao, D.; Wang, X. H.; Wu, Q.; Cao, Y.; Tu, J. C. *ACS Appl. Mater. Interfaces.* **2021**, *13* (28), 33006−33014.
(8) Wang, L. F.; Zhu, W. Q.; Lu, W. B.; Shi, L. N.; Wang, R.; Pang, R. X.; Cao, Y. Y.; Wang, F.; Xu, X. H. *Biosens. Bioelectron.* **2019**, *142*, 111577.
(9) Zheng, Y. N.; Liang, W. B.; Yuan, Y. L.; Xiong, C. Y.; Xie, S.; Wang, H. J.; Chai, Y. Q.; Yuan, R. *Biosens. Bioelectron.* **2016**, *81*, 423−430.
(10) Cao, J. T.; Ma, Y.; Lv, J. L. u.; Ren, S. W.; Liu, Y. M. *Chem. Commun.* **2020**, *56* (10), 1513−1516.
(11) Zhang, Y.; Hao, N.; Zhou, Z.; Hua, R.; Qian, J.; Liu, Q.; Li, H. N.; Wang, K. *Chem. Commun.* **2017**, *53* (43), 5810−5813.
(12) Sun, G. Q.; Zhang, Y.; Kong, Q. K.; Zheng, X. X.; Yu, J. H.; Song, X. R. *Biosens. Bioelectron.* **2015**, *66*, 565−571.
(13) Zhang, Y. T.; Figueroa-Miranda, G.; Wu, C. T.; Willbold, D.; Offenhäusser, A.; Mayer, D. *Nanoscale.* **2020**, *12* (31), 16501−16513.
(14) Zhang, Y.; Ge, L.; Li, M.; Yan, M.; Ge, S. G.; Yu, J. H.; Song, X. R.; Cao, B. Q. *Chem. Commun.* **2014**, *50* (12), 1417−1419.
(15) Wang, J.; Long, J.; Liu, Z. H.; Wu, W. Z.; Hu, C. G. *Biosens. Bioelectron.* **2017**, *91*, 53−59.
(16) Wang, J.; Liu, Z. H.; Hu, C. G.; Hu, S. S. *Anal. Chem.* **2015**, *87* (18), 9368−9375.
(17) Liu, A. R.; Yin, K. F.; Mi, L.; Ma, M. Y.; Liu, Y. J.; Li, Y.; Wei, W.; Zhang, Y. J.; Liu, S. Q. *Anal. Chim. Acta* **2017**, *973*, 82−90.
(18) Weng, Q. H.; Zheng, X. N.; Zhang, S. Y.; Zhu, L. L.; Huang, Q. J.; Liu, P. H.; Li, X. F.; Kang, J.; Han, Z. Z. *J. Photochem. Photobiol., A* **2020**, *388*, 112200.
(19) Liu, X.; Bao, C. Z.; Shao, X. R.; Zhang, Y.; Zhang, N.; Sun, X.; Fan, D.; Wei, Q.; Ju, H. X. *New J. Chem.* **2020**, *44* (6), 2452−2458.
(20) Zhang, Y.; Yang, H. N.; Yu, Y. B.; Zhang, Y. *Theranostics.* **2022**, *12* (6), 2674−2686.
(21) Wang, Y. H.; Ge, S. G.; Zhang, L. N.; Yu, J. H.; Yan, M.; Huang, J. D. *Biosens. Bioelectron.* **2017**, *89*, 859−865.
(22) Qian, Y. R.; Feng, J. H.; Xu, R.; Fan, D. W.; Du, Y.; Ren, X.; Wei, Q.; Ju, H. X. *ACS Appl. Mater. Interfaces.* **2020**, *12* (14), 16662−16669.
(23) Pan, Q. G.; Yang, K. R.; Wang, G. L.; Li, D. D.; Sun, J.; Yang, B.; Zou, Z. Q.; Hu, W. B.; Wen, K.; Yang, H. *Chem. Eng. J.* **2019**, *372*, 399−407.
(24) Sun, W. T.; Yu, Y.; Pan, H. Y.; Gao, X. F.; Chen, Q.; Peng, L. M. *J. Am. Chem. Soc.* **2008**, *130* (4), 1124−1125.
(25) Fan, B. B.; Fan, Q.; Hu, L. L.; Cui, M.; Wang, X. Y.; Ma, H. M.; Wei, Q. *ACS Appl. Mater. Interfaces.* **2020**, *12* (1), 1877−1884.
(26) Han, Z. Z.; Liao, L. L.; Wu, Y. T.; Pan, H. B.; Shen, S. F.; Chen, J. Z. *J. Hazard. Mater.* **2012**, *217*−*218*, 100−106.
(27) Kang, Z.; Gu, Y. S.; Yan, X. Q.; Bai, Z. M.; Liu, Y. C.; Liu, S.; Zhang, X. H.; Zhang, Z.; Zhang, X. J.; Zhang, Y. *Biosens. Bioelectron.* **2015**, *64*, 499−504.
(28) Zhang, Y. F.; Wang, M. D.; Wang, Y. G.; Feng, J. H.; Zhang, Y.; Sun, X.; Du, B.; Wei, Q. *Biosens. Bioelectron.* **2019**, *126*, 23−29.
(29) Feng, J. H.; Li, Y. Y.; Gao, Z. Q.; Lv, H.; Zhang, X. B.; Fan, D. W.; Wei, Q. *Biosens. Bioelectron.* **2018**, *99*, 14−20.
(30) Zhang, W. G.; Liu, Y. M.; Guo, F.; Liu, J. M.; Yang, F. Q. *J. Mater. Chem. C* **2019**, *7* (45), 14098−14108.
(31) Yukird, J.; Kaminsky, C. J.; Chailapakul, O.; Rodthongkum, N.; Vachet, R. W. *J. Am. Soc. Mass Spectrom.* **2021**, *32* (7), 1780−1788.
(32) Li, R.; Chen, F. F.; Liu, H. Q.; Wang, Z. X.; Zhang, Z. T.; Wang, Y.; Cui, H.; Liu, W.; Zhao, X. Z.; Sun, Z. J.; Guo, S. S. *ACS Appl. Mater. Interfaces* **2018**, *10* (19), 16327−16334.
(33) Lin, S.; Ren, H.; Wu, Z.; Sun, L.; Zhang, X. G.; Lin, Y. M.; Zhang, K. H. L.; Lin, C. J.; Tian, Z. Q.; Li, J. F. *J. Energy Chem.* **2021**, *59*, 721−729.
(34) Liu, J. M.; Zhu, L. Q.; Xiang, S. S.; Wang, H. L.; Liu, H. C.; Li, W. P.; Chen, H. N. *ACS Sustainable Chem. Eng.* **2019**, *7* (19), 16927−16932.
(35) Shi, Z.; Liu, J. N.; Lan, H. X.; Li, X. Y.; Zhu, B. Y.; Yang, J. H. *J. Mater. Sci.: Mater. Electron.* **2019**, *30* (19), 17682−17692.
(36) Han, Q. Z.; Wang, R. Y.; Xing, B.; Zhang, T.; Khan, M. S.; Wu, D.; Wei, Q. *Biosens. Bioelectron.* **2018**, *99*, 493−499.
(37) Wang, H.; Bai, Y. S.; Zhang, H.; Zhang, Z. H.; Li, J. H.; Guo, L. *J. Phys. Chem. C* **2010**, *114* (39), 16451−16455.
(38) Zhou, Z. J.; Fan, J. Q.; Wang, X.; Sun, W. Z.; Zhou, W. H.; Du, Z. L.; Wu, S. X. *ACS Appl. Mater. Interfaces.* **2011**, *3* (7), 2189−2194.
(39) Sun, L. L.; Shen, K. M.; Zhang, J. B.; Wan, W. J.; Cao, W. J.; Wang, Z. J.; Guo, C. Z. *RSC Advances.* **2021**, *11* (51), 32135−32142.
(40) Lin, Y.; Kannan, P.; Zeng, Y. B.; Qiu, B.; Guo, L. H.; Lin, Z. Y. *Sens. Actuators B Chem.* **2019**, *283*, 138−145.
(41) Chen, C. L.; Wei, Y. L.; Yuan, G. Z.; Liu, Q. L.; Lu, R. R.; Huang, X.; Cao, Y.; Zhu, P. H. *Adv. Funct. Mater.* **2017**, *27* (31), 1701575.
(42) Yang, L. W.; Liu, X. Q.; Li, L. L.; Zhang, S.; Zheng, H. J.; Tang, Y. F.; Ju, H. X. *Biosens. Bioelectron.* **2019**, *142*, 111487.
(43) Li, P. P.; Cao, Y.; Mao, C. J.; Jin, B. K.; Zhu, J. J. *Anal. Chem.* **2019**, *91* (2), 1563−1570.
(44) Fu, X. H.; Xu, K.; Feng, X. R. *Anal. Methods.* **2016**, *8* (5), 958−961.
(45) Xiao, K.; Wang, K.; Qin, W. J.; Hou, Y. F.; Lu, W. T.; Xu, H.; Wo, Y.; Cui, D. X. *Talanta* **2017**, *164*, 463−469.
(46) Amani, J.; Maleki, M.; Khoshroo, A.; Sobhani-Nasab, A.; Rahimi-Nasrabadi, M. *Anal. Biochem.* **2018**, *548*, 53−59.
(47) Li, H.; Xiao, Q. Y.; Lv, J. X.; Lei, Q.; Huang, Y. J. *Anal. Biochem.* **2017**, *531*, 48−55.
(48) Zhang, Y.; Liu, D. L.; Zhang, Y. Y.; Qian, Y. R.; Li, C. C.; Qu, Z. F.; Xu, R.; Wei, Q. *Biosens. Bioelectron.* **2022**, *203*, 114047.

https://doi.org/10.1021/acs.analchem.1c05577
Anal. Chem. 2022, 94, 6996−7003